Dual-doped graphene/perovskite bifunctional catalysts and the oxygen reduction reaction

Molina-García, Miguel A.; Rees, Neil V.

DOI:
10.1016/j.elecom.2017.10.004

Document Version
Publisher's PDF, also known as Version of record

Citation for published version (Harvard):
Molina-García, MA & Rees, NV 2017, 'Dual-doped graphene/perovskite bifunctional catalysts and the oxygen reduction reaction', *Electrochemistry Communications*, vol. 84, pp. 65-70.
https://doi.org/10.1016/j.elecom.2017.10.004

Electrochemistry Communications 84 (2017) 65–70

Contents lists available at ScienceDirect

Electrochemistry Communications

journal homepage: www.elsevier.com/locate/elecom

Dual-doped graphene/perovskite bifunctional catalysts and the oxygen reduction reaction

Miguel A. Molina-García, Neil V. Rees*

Centre for Doctoral Training in Fuel Cells and their Fuels, School of Chemical Engineering, University of Birmingham, Edgbaston, Birmingham B15 2TT, UK

ARTICLE INFO

Keywords:
Oxygen reduction reaction
Dual-doped graphene
Rotating-ring disk electrode
Metal-free catalyst
Perovskite
Peroxide formation

ABSTRACT

We report the first investigation of dual-doped graphene/perovskite mixtures as catalysts for oxygen reduction. Pairwise combinations of boron, nitrogen, phosphorus and sulfur precursors were co-reduced with graphene oxide and mixed with $La_{0.8}Sr_{0.2}MnO_3$ (LSM) to produce SN-Gr/LSM, PN-Gr/LSM and BN-Gr/LSM catalysts. In addition, the dual-doped graphenes, graphene, LSM, and commercial Pt/C were used as controls. The addition of LSM to the dual-doped graphenes significantly improved their catalytic performance, with optimised composition ratios enabling PN-Gr/LSM to achieve 85% of the current density of commercial Pt/C at − 0.6 V (vs. Ag/AgCl) at the same loading. The effective number of electrons increased to ca. 3.8, and kinetic analysis confirms the direct 4 electron pathway is favoured over the stepwise (2e + 2e) route: the rate of peroxide production was also found to be lowered by the addition of LSM to less than 10%.

1. Introduction

Research effort continues to focus on the oxygen reduction reaction (ORR) due to its importance in energy device applications (e.g., fuel cells and metal-air batteries) and, in particular, the search for more abundant and inexpensive catalyst replacements for the Pt-group materials is attracting increasing attention [1–3]. Amongst several candidates, perovskites have been demonstrated to be catalytically active [4–9]. However, the low conductivity typical of perovskites limits their application as single catalysts for the ORR [10].

In addition, graphene-related materials have also been considered due to its high conductivity and possibility of increasing the catalytic activity by the addition of dopant elements [11]. Specifically, dual-doped graphene with B, P or S in combination with N have been demonstrated to be catalytically active towards the oxygen reduction [12,13]. The combination of perovskites with highly conductive carbon materials have been previously reported for acetylene black [14], Vulcan carbon powder [15,16], Sibunit carbon [17], graphene [18,19], and even N-doped graphene [20,21], with varying results. The role of the carbon on the perovskite performance is still unclear. It has been proposed that the presence of carbon greatly improves the conductivity through the catalyst composite [22], whereas other workers suggest an influence of the carbon material on the ORR pathway [14,15]. In particular, the ORR can proceed in alkaline media via two different suggested mechanisms: either direct reduction of O_2 to OH^- by a 4-electron mechanism (Eq. (1)), or a 2-step process in which the O_2 is partially reduced to peroxide in a 2-electron mechanism (Eq. (2)) followed by either further reduction to OH^- [Eq. (3)] or decomposition of peroxide (Eq. (4)) [23].

$$O_2 + 2H_2O + 4e^- \xrightarrow{k_1} 4OH^- \quad (1)$$

$$O_2 + H_2O + 2e^- \xrightarrow{k_2} HO_2^- + OH^- \quad (2)$$

$$HO_2^- + H_2O + 2e^- \xrightarrow{k_3} 3OH^- \quad (3)$$

$$2HO_2^- \rightarrow O_2 + 2OH^- \quad (4)$$

Here, we investigate combining dual-doped graphenes with a perovskite for the first time. These materials exhibit improved electrocatalytic activity due to the synergic effects of the dual-doped graphene/perovskite, and optimisation of the composition obtains the best performance in terms of both current densities and number of electrons transferred in the ORR yields results that approach that of Pt/C.

2. Experimental

The dual-doped graphene catalysts were prepared via a thermal annealing of a mixture formed by graphene oxide (GO, Nanoinnova Inc., prepared by Hummers method, impurities measured by XRF: 0.7% Mn, 0.05% Fe, 0.03% W, 0.02% Zn, 0.02% Cr), and the precursors of the different doping agents. These were: boric acid (Sigma Aldrich, ≥ 99.5%), melamine (Aldrich, 99%), orthophosphoric acid (Fisher

* Corresponding author.
E-mail address: n.rees@bham.ac.uk (N.V. Rees).

http://dx.doi.org/10.1016/j.elecom.2017.10.004
Received 15 August 2017; Received in revised form 4 October 2017; Accepted 4 October 2017
Available online 05 October 2017

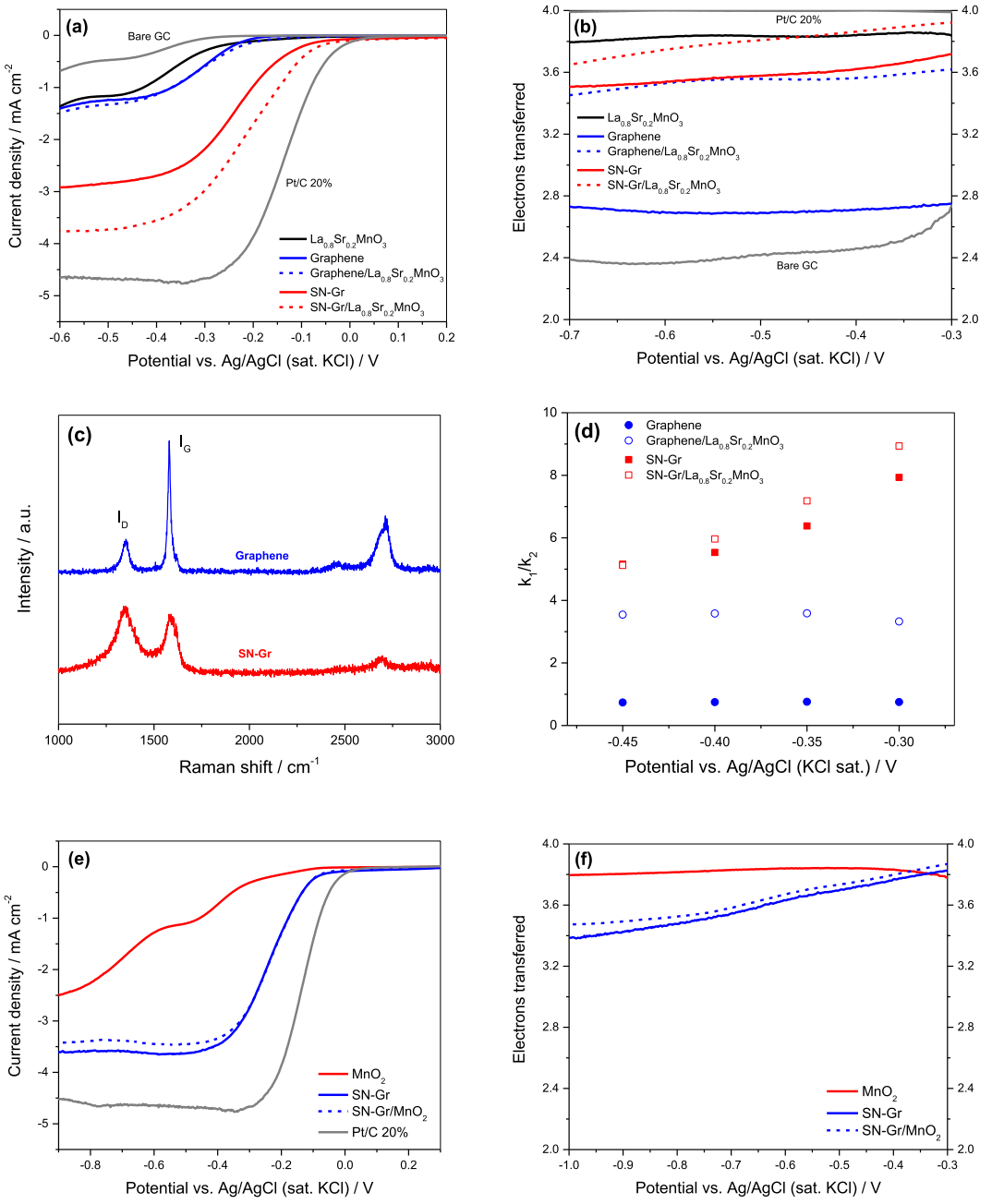

Fig. 1. (a) LSV of graphene and SN-Gr with and without perovskite in O_2-saturated 0.1 M KOH (measured at 10 mV s^{-1} scan rate and 1600 rpm, (doped)-graphene/LSM composites ratio 0.8:0.2, catalyst loading: 0.3 mg cm^{-2}). (b) Number of electrons transferred vs. potential obtained from RRDE measurements (ring potential fixed at + 0.5 V). (c) Raman spectra of pure graphene and SN-Gr. (d) k_1/k_2 ratios vs. potential (vs. sat. Ag/AgCl). (e) LSV of MnO_2, SN-Gr and combined SN-Gr/ MnO_2 in O_2-saturated 0.1 M KOH (measured at 10 mV s^{-1} scan rate and 1600 rpm, SN-Gr/MnO_2 composites ratio 0.8:0.2, catalyst loading: 0.4 mg cm^{-2}). (f) Number of electrons transferred vs. potential obtained from RRDE measurements (ring potential fixed at + 0.5 V).

Scientific, 86.75%) and dibenzyl disulfide (Aldrich, 98%). 100 mg of GO was mixed with 500 mg of melamine and 100 mg of the corresponding second precursor in 30 mL of ultrapure water (resistivity ≥ 18.2 MΩ cm, milli-Q Millipore). The ink was sonicated (Ultrawave, 50 Hz) for 1 h, then stirred for 15 h and centrifuged at 20000 rpm for 10 min. The supernatant was discarded and the resulting ink placed in an alumina crucible and pyrolised in a quartz tubular furnace at 900 °C for 2 h, heating rate of 5 °C min^{-1}, under 50 mL min^{-1} N_2 atmosphere (BOC gases, O_2 free, 99.998% purity). Finally, the sample was cooled under nitrogen before being weighed.

Rotating ring-disk voltammetry was performed using a Metrohm AutoLAB PGSTAT128N potentiostat connected to a rotator (Pine Instruments Inc., USA) in a Faraday cage. The reference electrode was an Ag/AgCl (sat. KCl) electrode (ALS Inc., E^0 = + 0.197 V vs. SHE) and the counter electrode was a Pt mesh. The RRDE (Pine Instruments Inc., USA) consisted of a GC disk (5.61 mm diameter) and a Pt ring with an area of 0.1866 cm^2, with a collection efficiency of 37%. Prior to each experiment the RRDE was thoroughly polished with consecutive alumina slurries of 1, 0.3 and 0.05 μm (Buehler) and then sonicated to remove any impurities. The catalyst inks were prepared by dispersing different amounts of the as-prepared dual-doped graphene (or pure graphene sourced from PiKem Ltd.), and $La_{0.8}Sr_{0.2}MnO_3$ (LSM, PRAXAIR Surf. Tech., surface area: 4.19 m^2 g^{-1}) or manganese (IV) oxide (MnO_2, Sigma-Aldrich, 99%), to give a total amount of 5 mg (with the desired composition) in 0.2 mL of isopropyl alcohol (VWR Chemicals), 0.78 mL of ultrapure water and 0.02 mL of 10 wt% Nafion

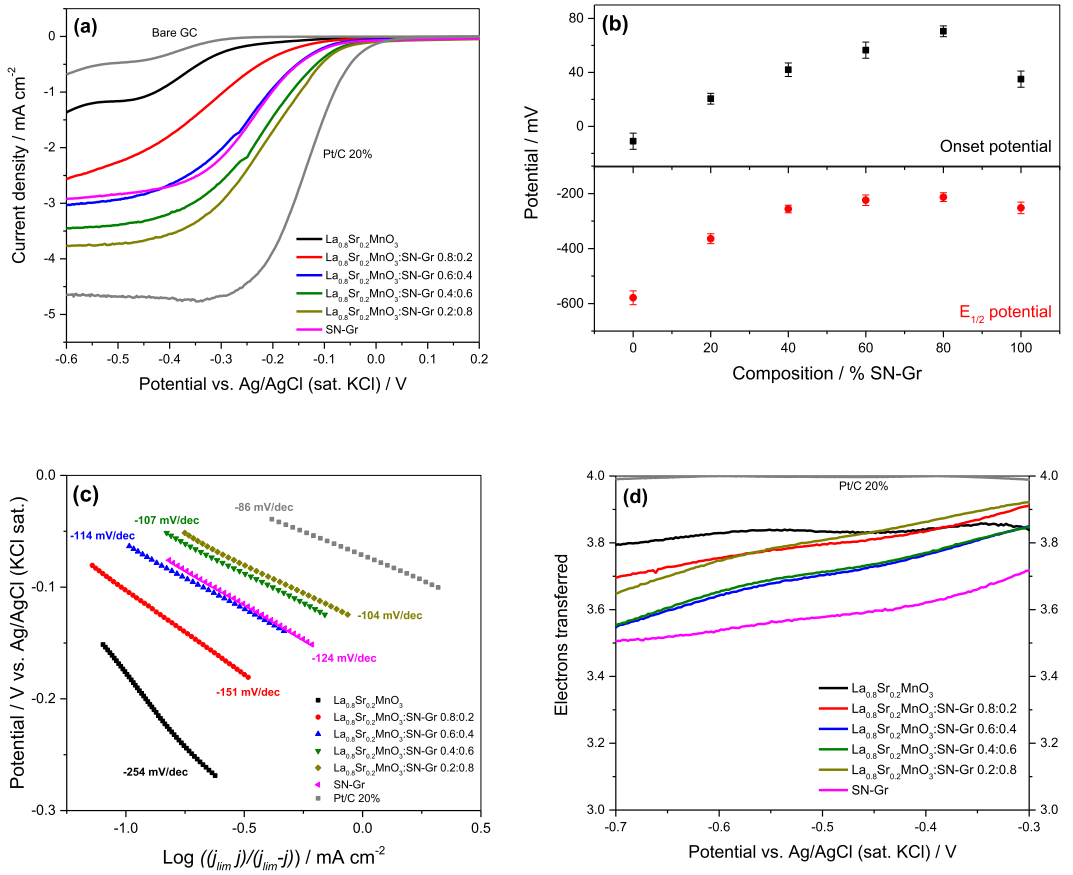

Fig. 2. (a) LSV of SN-Gr/perovskite at different compositions in O_2-saturated 0.1 M KOH. (b) Onset and half-current potentials vs. composition. (c) Tafel plots of the catalysts. (d) Number of transferred electrons calculated from RRDE measurements.

(Ion Power Inc.). This mixture was sonicated for 1 h and then a 15 μL aliquot was pipetted onto the GC disk to give a catalyst loading of 0.3 mg cm^{-2}. The droplet was left to dry at room temperature for 60 min at 400 rpm as described in literature [24] in order to get an uniform layer. The RRDE was then immersed in the O_2-saturated (BOC gases, N5, 99.999% purity) 0.1 M KOH (Sigma-Aldrich, 99.99%) alkaline solution and cycled between + 0.4 and − 1.0 V at 100 mV s^{-1} until a stable response was observed. Linear sweep voltammograms (LSV) were then recorded at 10 mV s^{-1} between + 0.4 and − 1.0 V at rotation speeds from 400 to 2400 rpm. The Pt ring voltage was fixed at + 0.5 V to ensure complete HO_2^- decomposition. The AC impedance spectra were also measured via a Metrohm Autolab FRA32M analyser between 500 kHz and 0.1 Hz at 0 V vs. Ag/AgCl (KCl sat.) with a signal amplitude of 10 mV. All measurements were carried out at 293 ± 1 K.

XRD measurements were obtained using a PANalytican Empyrean Pro X-ray powder diffractometer with a non-monochromated Cu X-ray source. Raman spectra were recorded using a Raman Microscope Renishaw inVia system (laser wavelength of 532 nm). X-ray photoelectron spectroscopy (XPS) spectra were obtained at the National EPSRC XPS Users' Service (NEXUS) at Newcastle University using a Thermo Scientific K-Alpha XPS instrument with a monochromatic Al Kα X-ray source.

3. Results and discussion

3.1. Comparison of dual-doped graphene/perovskite with graphene/perovskite catalysts

First, rotating ring-disk voltammetry was performed on a range of catalyst inks in an oxygen-saturated solution of 0.1 M KOH to determine the effect of the addition of LSM to the graphene derivatives. Due to the ORR in alkaline media being a multi-step process and that the graphene deposit creating a porous catalyst surface/layer, the number of electrons involved in the electrochemical reaction, *n*, should not be calculated from the application of Koutecky-Levich analysis to RDE measurements [25–28]. Therefore, in the present work the value of *n* is calculated from RRDE measurements using Eq. (5) [29]:

$$n = \frac{4I_D}{I_D + \left(\frac{I_R}{N}\right)} \quad (5)$$

where *n* is the number of electrons transferred, I_D the current measured at the GC disk ($I_D(H_2O) + I_D(H_2O_2)$), I_R the current measured at the Pt ring (related to the oxidation of H_2O_2) and *N* the collection efficiency which is a design parameter provided by the RRDE manufacturer ($N = 0.37$).

The addition of LSM to pure graphene increases the observed value of *n* from 2.7 to 3.6 (at − 0.5 V) although does not affect current density (Fig. 1a and b). In the case of sulfur and nitrogen-doped graphene, SN-Gr/LSM shows a significant improvement in both the measured current and the value of *n* compared to SN-Gr (from 3.6 to 3.8 at − 0.5 V). The source of this improvement has been postulated to be either conductivity effects [22], or the acceleration of Eq. (3) by the perovskite (since graphene materials tend to have lower *n* values due to catalysis of the 2e pathway) [30].

XRD and Raman spectroscopy were used to investigate the doped graphenes: both pure graphene and SN-Gr showed diffraction peaks at 26.5° corresponding to a basal inter-layer spacing of 0.34 nm typical of graphene materials [31]. The defects created during thermal annealing are believed to influence the conductivity of graphene materials [32], and modify the relative intensity of the I_D and I_G peaks in the Raman

spectra (Fig. 1c) observed at 1340 and 1580 cm^{-1}, respectively [33]. The measured values of the I_D/I_G ratio are 0.25 for graphene and 1.13 for SN-Gr, indicating fewer defects and thus higher conductivity for the graphene sample. AC impedance measurements of the high frequency resistances supported this ($39.7 \pm 0.1\ \Omega$ for graphene and $44.3 \pm 0.2\ \Omega$ for SN-Gr). The conclusion of this is that the positive effect observed for the SN-Gr/LSM (over Graphene/LSM) is not related to an increase in the conductivity of the material.

Next, the RRDE data was analysed using the method of Hsueh and Chin [34] to determine the ratio of rate constants k_1/k_2 (see Eqs. (1)–(3) above). Fig. 1d indicates that the addition of LSM promotes the direct 4e pathway over the stepwise 2e pathway in both cases (Gr/LSM and SN-Gr/LSM).

In order to see if the results obtained for the doped-graphene/perovskite catalyst are mainly due to the presence of Mn in the perovskite, an experiment comparing the catalytic activities of MnO_2, SN-Gr and SN-Gr/MnO_2 has been carried out and the results are shown in Fig. 1e and f. Unlike the results reflected in Fig. 1a, the addition of MnO_2 to the dual-doped graphene does not improve the current density nor the observed overpotential with respect to the doped-graphene alone. This suggests that the catalytic activity of the perovskite/doped-graphene hybrid catalyst does not come from the Mn activity only.

3.2. Optimization of composition

Next, the influence of the composition of the SN-Gr/LSM system on the catalytic performance towards the ORR was investigated by conducting analogous experiments on a series of SN-Gr/LSM composites (shown in Fig. 2). A gradual decrease in overpotential is observed as the SN-Gr content rises, reaching a minimum at 80% SN-Gr content (Fig. 2a). This echoes the trend in onset and half-wave potentials shown in Fig. 2b, with the most positive onset being + 70.5 mV and the least negative half-wave potential being − 213 mV at 80% SN-Gr content.

Tafel plots (Fig. 2c) confirm the same trend, showing the SN-Gr/LSM 0.8:0.2 the lowest value of Tafel slope with $-104\ mV\ dec^{-1}$ (for comparison the same value obtained for Pt/C 20% was $-86\ mV\ dec^{-1}$). The values of n calculated from ring currents are provided in Fig. 2d and show that LSM reaches a maximum value of n (at − 0.5 V) of 3.8, whereas the lowest value of 3.6 corresponds to pure dual-doped graphene. For mixed SN-Gr/LSM composites n does not vary systematically between these two values, with n equal to 3.8 for 20 and 80% dual-doped graphene composition and 3.7 for 40 and 60%. This points to that the ORR takes place in the pure perovskite by a 4e mechanism, although this selectivity towards the direct O_2 reduction into OH^- is not reflected in improved current densities, probably due to the previously mentioned poor conductivity of perovskites. The ORR performance of LSM perovskite is improved with the addition of dual-doped graphene, the best results being obtained at higher SN-Gr contents.

The principal conclusion is that the electrochemical performance mainly comes from the intrinsic catalytic activity of the doped-graphene, with the perovskite playing a role of further reducing agent of the peroxide produced by the graphene catalyst. It has been proposed that the carbon facilitates the reduction of O_2 into HO_2^- in a $2e^-$ pathway and the perovskite assists the reduction of HO_2^- into OH^- to give an overall (2e + 2e) mechanism [10]. In this case, it can be observed that the SN-dual doped graphene shows a value of $n = 3.6$ when it is not combined with perovskite, which increases on the addition of perovskite to around 3.8 (comparable with n for ORR on the pure LSM itself). This explanation is therefore possible if the rate of the perovskite-facilitated peroxide reduction is fast compared to the formation of peroxide.

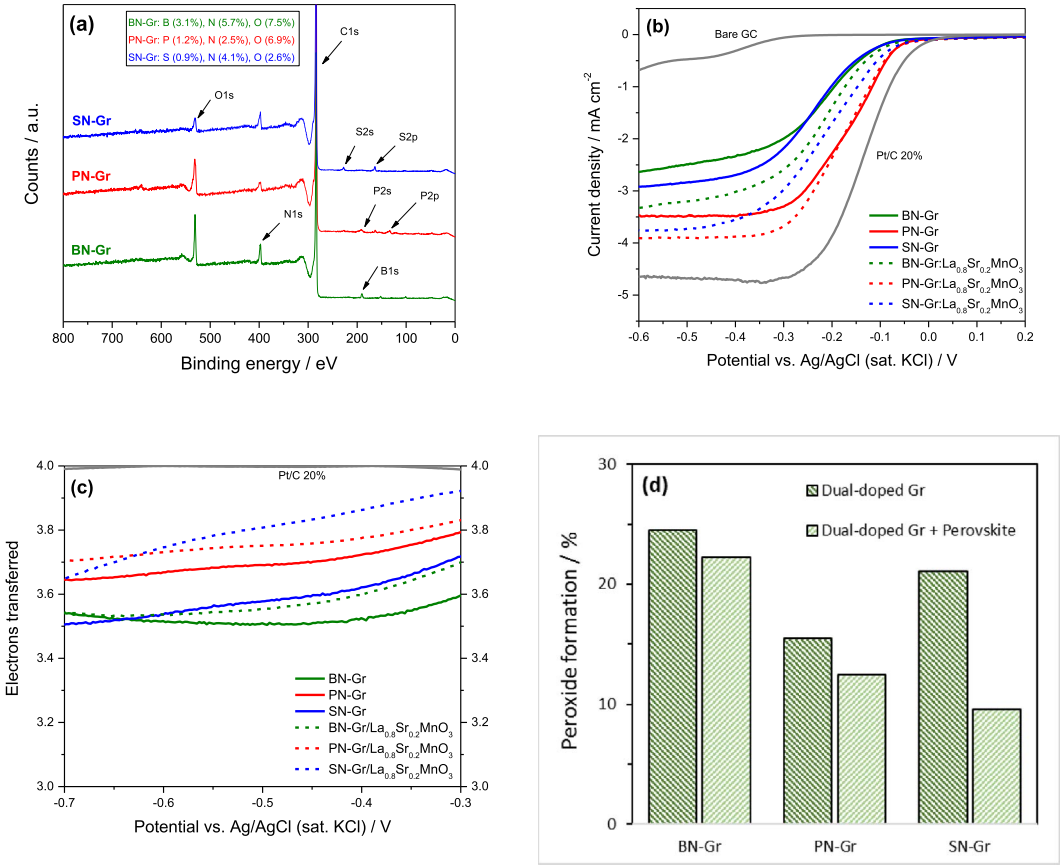

Fig. 3. (a) Survey XPS spectra of the dual-doped graphenes. (b) LSV of the dual-doped graphenes with and without 20% perovskite addition at different compositions in O_2-saturated 0.1 M KOH. (c) Number of electrons transferred vs. potential. (d) Mole fraction (in %) of produced peroxide obtained from RRDE measurements.

3.3. Comparison of different dual-doped graphenes combined with perovskite oxides

In order to elucidate if the conclusions obtained for SN-Gr/LSM could be extended to other dual-doped graphenes, graphene doped with boron-nitrogen (BN-Gr) and phosphorus-nitrogen (PN-Gr) were tested under the same conditions. Their compositions were determined via XPS and are shown in the inset of Fig. 3a. The voltammetry in Fig. 3b illustrates that all the doped-graphenes increased their limiting current densities when 20% perovskite was added. The PN-Gr catalyst exhibited the highest activity, which is further enhanced by the addition of perovskite such that its current density approaches commercial Pt/C.

In all cases the addition of LSM caused an increase in the value of *n* (Fig. 3c), with particular interest in SN-Gr where *n* rises from 3.6 to 3.8. The production rate of peroxide intermediates (Fig. 3d) drops from 21.1% for the dual-doped SN-Gr to 9.6% for SN-Gr/LSM. This is an unusually low value for a Pt-free catalyst.

It has been proposed that the carbon could affect the electronic structure of B-site transition metal of perovskite [10]. Some authors have demonstrated that the addition of carbon to perovskites can modify the oxidation state of the B-site transition metal, for example Co, which is linked to enhanced catalytic activity [35], although this was not observed for Fe [36]. The possible interaction between the heteroatoms of doped-graphene with the electronic structure of B-site transition metal of perovskite, and its possible relation with the enhanced catalytic performance, will be investigated in a separate study to elucidate further these effects on the catalytic mechanism of these promising hybrid materials.

4. Conclusions

The combination of a perovskite (LSM) with dual-doped graphenes shows a synergistic effect towards the ORR, with an optimal composition of 20% perovskite yielding a value of *n* of 3.8 for SN-Gr/LSM, whereas the PN-Gr/LSM develops the highest catalytic activity approaching that of commercial Pt/C catalyst with the *same* catalyst loading. The addition of LSM further favours the 4e mechanism over the stepwise 2e + 2e pathway, and the increase of conductivity to LSM provided by the graphene derivative is found not to be significant in the catalytic behaviour.

Acknowledgments

We thank the EPSRC for funding through grant no. EP/G037116/1.

References

[1] L. Dai, Y. Xue, L. Qu, H.J. Choi, J.B. Baek, Metal-free catalysts for oxygen reduction reaction, Chem. Rev. 115 (2015) 4823–4892, http://dx.doi.org/10.1021/cr5003563.

[2] A. Morozan, B. Jousselme, S. Palacin, Low-platinum and platinum-free catalysts for the oxygen reduction reaction at fuel cell cathodes, Energy Environ. Sci. 4 (2011) 1238, http://dx.doi.org/10.1039/c0ee00601g.

[3] F. Jaouen, E. Proietti, M. Lefèvre, R. Chenitz, J.-P. Dodelet, G. Wu, H.T. Chung, C.M. Johnston, P. Zelenay, Recent advances in non-precious metal catalysis for oxygen-reduction reaction in polymer electrolyte fuel cells, Energy Environ. Sci. 4 (2011) 114, http://dx.doi.org/10.1039/c0ee00011f.

[4] M. Risch, Perovskite electrocatalysts for the oxygen reduction reaction in alkaline media, Catalysts. 7 (2017) 154, http://dx.doi.org/10.3390/CATAL7050154.

[5] J. Suntivich, H. a Gasteiger, N. Yabuuchi, H. Nakanishi, J.B. Goodenough, Y. Shao-Horn, Design principles for oxygen-reduction activity on perovskite oxide catalysts for fuel cells and metal-air batteries, Nat. Chem. 3 (2011) 546–550, http://dx.doi.org/10.1038/nchem.1069.

[6] J. Sunarso, A. a J. Torriero, W. Zhou, P.C. Howlett, M. Forsyth, Oxygen reduction reaction activity of La-based perovskite oxides in alkaline medium: a thin-film rotating ring-disk electrode study, J. Phys. Chem. C 116 (2012) 5827–5834, http://dx.doi.org/10.1021/jp211946n.

[7] T. Poux, A. Bonnefont, A. Ryabova, G. Kéranguéven, G.A. Tsirlina, E.R. Savinova, Electrocatalysis of hydrogen peroxide reactions on perovskite oxides: experiment versus kinetic modeling, Phys. Chem. Chem. Phys. 16 (2014) 13595–13600 (doi: 10.1039/c4cp00341a).

[8] D. Chen, C. Chen, Z. Zhang, Z.M. Baiyee, F. Ciucci, Z. Shao, Compositional engineering of perovskite oxides for highly efficient oxygen reduction reactions, ACS Appl. Mater. Interfaces 7 (2015) 8562–8571, http://dx.doi.org/10.1021/acsami.5b00358.

[9] Y. Zhu, W. Zhou, J. Yu, Y. Chen, M. Liu, Z. Shao, Enhancing electrocatalytic activity of perovskite oxides by tuning cation deficiency for oxygen reduction and evolution reactions, Chem. Mater. 28 (2016) 1691–1697, http://dx.doi.org/10.1021/acs.chemmater.5b04457.

[10] Y. Zhu, W. Zhou, Z. Shao, Perovskite/carbon composites: applications in oxygen electrocatalysis, Small 13 (2017) 1603793, , http://dx.doi.org/10.1002/smll.201603793.

[11] Y. Jiao, Y. Zheng, M. Jaroniec, S.Z. Qiao, Origin of the electrocatalytic oxygen reduction activity of graphene-based catalysts: a roadmap to achieve the best performance, J. Am. Chem. Soc. 136 (2014) 4394–4403, http://dx.doi.org/10.1021/ja500432h.

[12] C.H. Choi, S.H. Park, S.I. Woo, Binary and ternary doping of nitrogen, boron, and phosphorus into carbon for enhancing electrochemical oxygen reduction activity, ACS Nano 6 (2012) 7084–7091, http://dx.doi.org/10.1021/nn3021234.

[13] H. Zhang, X. Liu, G. He, X. Zhang, S. Bao, W. Hu, Bioinspired synthesis of nitrogen/sulfur co-doped graphene as an efficient electrocatalyst for oxygen reduction reaction, J. Power Sources 279 (2015) 252–258, http://dx.doi.org/10.1016/j.jpowsour.2015.01.016.

[14] E. Fabbri, R. Mohamed, P. Levecque, O. Conrad, R. Kötz, T.J. Schmidt, Composite electrode boosts the activity of $Ba_{0.5}Sr_{0.5}Co_{0.8}Fe_{0.2}O_{3-\delta}$ perovskite and carbon toward oxygen reduction in alkaline media, ACS Catal. 4 (2014) 1061–1070, http://dx.doi.org/10.1021/cs400903k.

[15] X. Li, W. Qu, J. Zhang, H. Wang, Electrocatalytic activities of $La_{0.6}Ca_{0.4}CoO_3$ and $La_{0.6}Ca_{0.4}CoO_3$-carbon composites toward the oxygen reduction reaction in concentrated alkaline electrolytes, J. Electrochem. Soc. 158 (2011) A597, http://dx.doi.org/10.1149/1.3560170.

[16] V. Hermann, D. Dutriat, S. Müller, C. Comninellis, Mechanistic studies of oxygen reduction at $La_{0.6}Ca_{0.4}CoO_3$-activated carbon electrodes in a channel flow cell, Electrochim. Acta 46 (2000) 365–372, http://dx.doi.org/10.1016/S0013-4686(00)00593-4.

[17] T. Poux, A. Bonnefont, G. Kéranguéven, G.A. Tsirlina, E.R. Savinova, Electrocatalytic oxygen reduction reaction on perovskite oxides: series versus direct pathway, ChemPhysChem 15 (2014) 2108–2120, http://dx.doi.org/10.1002/cphc.201402022.

[18] J. Hu, L. Wang, L. Shi, H. Huang, Preparation of $La_{1-x}Ca_xMnO_3$ perovskite-graphene composites as oxygen reduction reaction electrocatalyst in alkaline medium, J. Power Sources 269 (2014) 144–151, http://dx.doi.org/10.1016/j.jpowsour.2014.07.004.

[19] J. Hu, L. Wang, L. Shi, H. Huang, Oxygen reduction reaction activity of $LaMn_{1-x}Co_xO_3$-graphene nanocomposite for zinc-air battery, Electrochim. Acta 161 (2015) 115–123, http://dx.doi.org/10.1016/j.electacta.2015.02.048.

[20] N.-I. Kim, R.A. Afzal, S.R. Choi, S.W. Lee, D. Ahn, S. Bhattacharjee, S.-C. Lee, J.H. Kim, J.-Y. Park, Highly active and durable nitrogen doped-reduced graphene oxide/double perovskite bifunctional hybrid catalysts, J. Mater. Chem. A 5 (2017) 13019–13031, http://dx.doi.org/10.1039/C7TA02283B.

[21] X. Ge, F.W.T. Goh, B. Li, T.S.A. Hor, J. Zhang, P. Xiao, X. Wang, Y. Zong, Z. Liu, Efficient and durable oxygen reduction and evolution of a hydrothermally synthesized $La(Co_{0.55}Mn_{0.45})_{0.99}O_{3-\delta}$ nanorod/graphene hybrid in alkaline media, Nano 7 (2015) 9046–9054, http://dx.doi.org/10.1039/C5NR01272D.

[22] T. Poux, F.S. Napolskiy, T. Dintzer, G. Kéranguéven, S.Y. Istomin, G.A. Tsirlina, E.V. Antipov, E.R. Savinova, Dual role of carbon in the catalytic layers of perovskite/carbon composites for the electrocatalytic oxygen reduction reaction, Catal. Today 189 (2012) 83–92, http://dx.doi.org/10.1016/j.cattod.2012.04.046.

[23] X. Ge, A. Sumboja, D. Wuu, T. An, B. Li, F.W.T. Goh, T.S.A. Hor, Y. Zong, Z. Liu, Oxygen reduction in alkaline media: from mechanisms to recent advances of catalysts, ACS Catal. 5 (2015) 4643–4667, http://dx.doi.org/10.1021/acscatal.5b00524.

[24] Y. Garsany, I.L. Singer, K.E. Swider-Lyons, Impact of film drying procedures on RDE characterization of Pt/VC electrocatalysts, J. Electroanal. Chem. 662 (2011) 396–406, http://dx.doi.org/10.1016/j.jelechem.2011.09.016.

[25] S. Treimer, A. Tanga, D. Johnson, Consideration of the application of Koutecky-Levich plots in the diagnoses of charge-transfer mechanisms at rotated disk electrodes, Electroanalysis 14 (2002) 165–171.

[26] R. Zhou, Y. Zheng, M. Jaroniec, S.-Z. Qiao, Determination of the electron transfer number for the oxygen reduction reaction: from theory to experiment, ACS Catal. 6 (2016) 4720–4728, http://dx.doi.org/10.1021/acscatal.6b01581.

[27] J. Masa, C. Batchelor-McAuley, W. Schuhmann, R.G. Compton, Koutecky-Levich analysis applied to nanoparticle modified rotating disk electrodes: electrocatalysis or misinterpretation, Nano Res. 7 (2014) 71–78, http://dx.doi.org/10.1007/s12274-013-0372-0.

[28] S.V. Sokolov, L. Sepunaru, R.G. Compton, Taking cues from nature: hemoglobin catalysed oxygen reduction, Appl. Mater. Today. 7 (2017) 82–90, http://dx.doi.org/10.1016/j.apmt.2017.01.005.

[29] E. Claude, T. Addou, J. Latour, P. Aldebert, A new method for electrochemical screening based on the rotating ring disc electrode and its application to oxygen reduction catalysts, J. Appl. Electrochem. 28 (1998) 57–64 (doi: 10.1023/A:1003297718146).

[30] M.A. Molina-García, N.V. Rees, Effect of catalyst carbon supports on the oxygen reduction reaction in alkaline media: a comparative study, RSC Adv. 6 (2016) 94669–94681, http://dx.doi.org/10.1039/C6RA18894J.

[31] Z. Sheng, L. Shao, J. Chen, W. Bao, F. Wang, X. Xia, Catalyst-free synthesis of nitrogen-doped graphene via thermal annealing graphite oxide with melamine and its

excellent electrocatalysis, ACS Nano 5 (2011) 4350–4358, http://dx.doi.org/10.1021/nn103584t.
[32] R. Beams, L.G. Canç Ado, L. Novotny, Raman characterization of defects and dopants in graphene, J. Phys. Condens. Matter 27 (2015) 83002, , http://dx.doi.org/10.1088/0953-8984/27/8/083002.
[33] L. Niu, Z. Li, W. Hong, J. Sun, Z. Wang, L. Ma, J. Wang, S. Yang, Pyrolytic synthesis of boron-doped graphene and its application aselectrode material for supercapacitors, Electrochim. Acta 108 (2013) 666–673, http://dx.doi.org/10.1016/j.electacta.2013.07.025.
[34] K.L. Hsueh, D.T. Chin, S. Srinivasan, Electrode kinetics of oxygen reduction. A theoretical and experimental analysis of the rotating ring-disk electrode method, J. Electroanal. Chem. Interfacial Electrochem. 153 (1983) 79–95, http://dx.doi.org/10.1016/0368-1874(83)80358-x.
[35] O. Haas, F. Holzer, S. Müller, J.M. McBreen, X.Q. Yang, X. Sun, M. Balasubramanian, X-ray absorption and diffraction studies of $La_{0.6}Ca_{0.4}CoO_3$ perovskite, a catalyst for bifunctional oxygen electrodes, Electrochim. Acta 47 (2002) 3211–3217, http://dx.doi.org/10.1016/S0013-4686(02)00241-4.
[36] E. Fabbri, M. Nachtegaal, X. Cheng, T.J. Schmidt, Superior bifunctional electrocatalytic activity of insight into the local electronic structure, Adv. Energy Mater. 5 (2015) 1–5 (doi: 10.1002/aenm.201402033).